Protein network centralities as descriptor for QM region construction in QM/MM simulations of enzymes

Felix Brandt, Christoph R. Jacob[1]

Technische Universität Braunschweig, Institute of Physical and Theoretical Chemistry,
Gaußstraße 17, 38106 Braunschweig, Germany

Supporting Information

Date: July 10, 2023

[1]E-Mail: c.jacob@tu-braunschweig.de

Contents

S1 Computational Details **3**

S2 Additional data for COMT **5**

S3 Results and additional data for TIM **11**

List of Tables

S1 Comparison of residue ranks for COMT 6

S2 PCVA-constructed QM regions of increasing size for COMT 8

S3 16-residue QM regions for COMT 9

S4 Residues detected by betweenness centrality for different simulation times . 10

S5 Comparison of residue ranks for TIM 13

S6 Different-sized PCVA-constructed QM regions for TIM 15

S7 16-residue QM regions for TIM 16

List of Figures

S1 VDD charges and reaction energies for TIM 12

S1 Computational Details

The initial structures for QM/MM calculations were generated according to the following protocols in our previous work [1, 2]. Molecular dynamics (MD) calculations were performed using GROMACS 2019.3 [3, 4] with the AMBER99SB-ILDN [5] force field. The different substrates were parametrized using ANTECHAMBER [6, 7] and ACPYPE [8, 9].

For COMT the equilibrated initial reactant and product structures provided by Kulik *et al.* [10] were solvated in TIP3P [11] water molecules in a cubic simulation box with 1 nm distance from the enzyme to the borders. After neutralizing the system by adding six sodium cations the solvent molecules and ions were minimized with the enzyme structure held fixed. Finally, a spherical droplet with a radius of 33 Å from the COMT center of mass was extracted containing COMT with substrates, sodium ions and the corresponding water molecules as starting structure for the QM/MM calculations.

The TIM reactant and product structures were prepared starting from the monomer A of the crystal structure with co-crystallized inhibitor phosphoglycolohydroxamic acid (PGH) (PDB: 7TIM [12]) by modification of PGH to dihydroxyacetone phosphate (DHAP) and glyceraldehyde phosphate (GAP), respectively. After solvating and neutralizing (3 sodium ions, protocol see COMT) the structure was minimized and equilibrated in an NVT and NPT ensemble, respectively.

All QM/MM calculations for atom-economical QM regions were performed using the Amsterdam Modeling Suite (AMS Version 2020.203) [13]. The Amsterdam Density Functional (ADF) engine [14] was used for the QM part applying density functional theory (DFT) with the PBE exchange-correlation functional [15] employing a DZ and a TZP Slater-type orbital basis set [16] for all geometry optimizations and single point calculations, respectively. In case of occurring convergence problems during the geometry optimizations (especially for TIM) the optimization was started using the B3LYP [17,18] XC functional

and afterwards continued with PBE. For the MM region the ForceField engine of AMS was used with the AMBER95 force field [19], which was extended by parameters for the substrates. The FIRE [20] minimization algorithm was used for all QM/MM geometry optimizations with all MM solvent molecules and ions fixed to their initial coordinates.

Input files for QM/MM were generated using the PDB2ADF tool provided provided by AMS. Electrostatic embedding as implemented in AMS [21] was applied for the interaction between the QM and MM regions. Link atoms were placed on the C_α–C and C_α–N bonds only including the α-carbon atom in the QM region for single QM amino acids, while also including the remaining backbone atoms between two subsequent QM amino acids to reduce the number of link atoms. All charges evaluated for the assessment of convergence and atom-economical QM regions are calculated from the Voronoi deformation density (VDD) [22] of the reactant structures only.

The construction of QM regions using saaPCVA results for COMT and TIM were generated following the corresponding protocols shown in our previous work (using the *standard* variant) [1, 2]. The PCVA QM regions used here are identical to those constructed previously. Residues included in the QM regions for each system are listed in Tables S2 and S3 for COMT and in Tables S6 and S7 for TIM. These tables also give the corresponding QM region charge and the number of atoms and link atoms.

For the calculation of centrality descriptors, molecular dynamics (MD) calculations were performed as described above. For both, COMT and TIM, the identical protocol was executed featuring the solvation in TIP3P water in a cubic simulation box with 1 nm distance from the enzyme to the borders and the neutralization with sodium ions followed by minimization, NVT and NPT equilibrations runs and finally the productive 100 ns MD simulation resulting in 10,000 frames as basis for graph construction.

The analysis of results was achieved with Python. Network analysis and centrality calcu-

lation were also performed in Python using the WISP script [23] for correlation matrix and contact map construction and the networkx module [24, 25] for calculating d-, b- and e-centralities. Plots were generated with MATPLOTLIB [26, 27] and structures were visualized using Visual Molecular Dynamics (VMD) [28].

S2 Additional data for COMT

The rankings of the amino acid residues generated using PCVA, the three different centrality descriptors, and with the mixed *b-half* and *b-norm* approaches are listed in Table S1.

The residues included in the QM regions of increasing size (used in Fig. 2 A/B) are listed in Table S2, the residues included in the atom-economial QM regions (used in Fig. 2 C/D) are listed in Fig. S3.

Table S1: Comparison of residues included in a 16-residue (17 for *d*-centrality) QM region of COMT using PCVA, using *d*-, *b*-, and *e*-centrality descriptors, and using the mixed *b-half* and *b-norm* approaches. Numbers indicate the rank of the amino acid according to different descriptors. The highest-ranked 16 residues are marked in red. Residues in the *d*-centrality ranking can have the same rank if they are assigned the same centrality value. For the mixed approaches, 16 residues are assigned to their detection method indicated by b for *b*-centrality and by p for PCVA.

Residue	PCVA	d	b	e	b-half	b-norm
ILE8	155	1	12	98	b	b
MET39	8	18	139	171	p	—
ASN40	25	93	20	110	—	—
VAL41	15	66	27	51	—	—
GLY42	53	110	104	86	—	—
LYS45	16	3	18	23	—	—
LEU62	52	28	13	20	—	b
GLU63	23	18	10	17	b	b
GLY65	2	132	21	105	p	p
ALA66	6	93	11	79	p	p
TYR67	14	28	6	99	b	b
TYR70	34	17	4	36	b	b
VAL73	138	9	7	35	b	b
ARG74	186	9	24	27	—	—
MET75	79	9	1	9	b	b
GLU89	7	46	22	117	p	—
MET101	113	3	29	65	—	—
ILE122	87	3	17	46	—	—
MET136	81	3	2	1	b	b
VAL137	48	46	26	10	—	—
PHE138	12	28	14	6	—	b
LEU139	13	66	50	16	—	—
ASP140	1	66	9	28	p	p
HIS141	5	110	71	68	p	p
TRP142	10	202	203	149	—	—

LYS143	11	66	64	52	—	—
TYR146	17	1	16	5	—	—
THR150	71	9	37	12	—	—
THR163	134	9	32	13	—	—
LEU165	56	18	15	3	—	—
LEU166	33	46	42	8	—	—
ALA167	19	46	67	7	—	—
ASP168	3	9	5	2	p	p
ASN169	4	3	8	11	p	p
VAL170	21	18	83	14	—	—
PRO173	24	202	198	160	—	—
PHE178	45	9	44	15	—	—
SER195	43	152	146	123	—	—
LEU197	27	66	48	100	—	—
GLU198	9	28	3	64	b	b
ASP204	29	28	69	49	—	—
GLY205	32	28	111	24	—	—
LEU206	30	46	78	26	—	—
GLU207	47	3	30	4	—	—
TYR211	192	9	34	37	—	—

Table S2: Information on the QM regions of increasing size for COMT constructed by PCVA with a variation of −0.5. Reproduced from *J. Chem. Theory Comput.* **18**, 2584-2596 (2022), DOI: 10.1021/acs.jctc.1c01093.

Region	Charge	Residues	Link atoms	Included residues
1	+1	0	0	MG SAM CAT
2’	0	3	6	D140 G65 D168 *
3’	-1	7	8	D140 G65 D168 N169 H141 A66 E89 *
4’	-1	13	12	D140 G65 D168 N169 H141 A66 E89 M39 E198 W142 K143 F138 L139 *
5’	0	19	18	D140 G65 D168 N169 H141 A66 E89 M39 E198 W142 K143 F138 L139 Y67 V41 K45 Y146 L64 A167 *
6’	0	22	22	D140 G65 D168 N169 H141 A66 E89 M39 E198 W142 K143 F138 L139 Y67 V41 K45 Y146 L64 A167 C172 V170 N91 *
7’	-1	26	22	D140 G65 D168 N169 H141 A66 E89 M39 E198 W142 K143 F138 L139 Y67 V41 K45 Y146 L64 A167 C172 V170 N91 E63 P173 N40 C94 *
8’	-2	34	24	D140 G65 D168 N169 H141 A66 E89 M39 E198 W142 K143 F138 L139 Y67 V41 K45 Y146 L64 A167 C172 V170 N91 E63 P173 N40 C94 L197 I90 D204 L206 G174 G205 L166 Y70 *
9’	-2	43	26	D140 G65 D168 N169 H141 A66 E89 M39 E198 W142 K143 F138 L139 Y67 V41 K45 Y146 L64 A167 C172 V170 N91 E63 P173 N40 C94 L197 I90 D204 L206 G174 G205 L166 Y70 R145 I88 A175 I171 D144 W37 S118 T87 S195 *

* + MG SAM CAT H_2O

Table S3: Information on the atom-economical, 16-residue QM regions for COMT constructed based on PCVA schemes, centrality descriptors and mixed approaches. Residues are ordered according to their position in the indicator ranking.

Region	Charge	Residues	Link atoms	Included residues
PCVA	0	16	16	D140 G65 D168 N169 H141 A66 E89 M39 E198 W142 K143 F138 L139 Y67 V41 K45 *
degree	1	17	28	Y146 I8 E207 N169 M136 I122 M101 K45 Y211 F178 D168 T163 T150 M75 R74 V73 Y70 *
between	-2	16	26	M75 M136 E198 Y70 D168 Y67 V73 N169 D140 E63 A66 I8 L62 F138 L165 Y146 *
eigenvector	-1	16	16	M136 D168 L165 E207 Y146 F138 A167 L166 M75 V137 N169 T150 T163 V170 F178 L139 *
half	-3	16	24	D140 G65 D168 N169 H141 A66 E89 M39 M75 M136 E198 Y70 Y67 V73 E63 I8 *
norm	-2	16	22	D140 G65 D168 N169 H141 M75 M136 E198 Y70 Y67 A66 V73 E63 I8 L62 F138 *

* + MG SAM CAT H_2O

To save computational time concerning the preceding MD simulation we investigated the composition of exclusively *b*-centrality-constructed QM regions with reducing the simulation time and consequently also the number of snapshots at the same time. Table S4 shows the ranks for the 16 highest-ranked residues in the full 100 ns simulation for all other truncated setups in a range between 90 and 10 ns in 10 ns steps. If we assume the longest simulation with the most snapshots to deliver the best results a 60 ns simulation would be sufficient as it only misses TYR146 by one rank. Consequently, the simulation time for this system to converge the centrality results is very short and together with the PCVA calculations the whole procedure can be executed in less than one day which still is faster compared to other established methods.

Table S4: The ranks for the 16 residues detected by the betweenness centrality approach in COMT based on a 100 ns MD simulation are shown for shorter simulation times ranging from 90 ns to 10 ns. Residues that are ranked under the first 16 amino acids are marked red.

Residue	100 ns	90 ns	80 ns	70 ns	60 ns	50 ns	40 ns	30 ns	20 ns	10 ns
MET75	1	1	1	1	1	1	1	1	6	9
MET136	2	2	2	2	3	4	3	2	22	21
GLU198	3	3	3	3	2	3	2	5	2	6
TYR70	4	4	4	4	4	2	6	7	9	2
ASP168	5	5	7	7	8	7	7	8	5	14
TYR67	6	6	6	6	6	8	8	9	4	4
VAL73	7	7	9	9	5	10	9	6	7	11
ASN169	8	8	8	8	12	9	10	10	12	7
ASP140	9	9	13	13	13	21	20	19	25	17
GLU63	10	10	10	10	10	19	19	27	18	26
ALA66	11	11	11	11	11	12	14	11	8	10
ILE8	12	12	14	14	16	15	13	15	16	25
LEU62	13	13	12	12	9	6	4	4	3	5
PHE138	14	14	5	5	7	5	5	3	1	1
LEU165	15	15	15	15	14	11	12	14	26	13
TYR146	16	17	16	16	17	22	18	18	31	29

S3 Results and additional data for TIM

For COMT, we have shown in the main that the using *b*-centrality descriptor combined with PCVA for the construction of atom-economical QM regions is able to push both ligand charges and reaction energies towards the best estimate. To verify this trend, we applied the analogous analysis to triosephosphate isomerase system (PDB: 7TIM), which we previously used as a test case for systematic QM region construction in Ref. 2.

We again generated centrality rankings for all three centrality descriptors based on the TIM molecular dynamics trajectory (see Table S5) and constructed atom-economical, 16-residue QM regions (see Table S7) based on these rankings and the *half* approach combining PCVA and the *b*-centrality ranking. The results for the ligand charges and reaction energies are shown in Fig. S1 (see lower part, C/D) in comparison to those for QM regions of increasing size constructed using PCVA (see upper part, A/B)

Regarding the DHAP ligand charge (see Fig. S1C), with a 16-residue QM region the standard PCVA approach severely underestimates the negative ligand charge (-0.1 for PCVA vs. the best estimate of -0.25). The *d*- and *e*-centrality yield a ligand charge of zero, while using the *b*-centrality pushes the charge in negative direction towards the best estimate. The *b-half* approach severely overestimates the negative energy, but overall the results indicate that applying the *b*-centrality descriptor is capable of shifting results into the right direction.

For the reaction energy, the 16-residue QM region constructed using standard PCVA yields a slightly negative reaction energy, i.e., this QM region is not adequate, which we attributed to an insufficient size of a 16-residue QM region for this particular system in our previous work [2]. Using the *d*-centrality, a similar result is obtained, while all other approaches shift the resulting reaction energy into the right direction, but with overestimation compared to our best estimate of 9.5 kcal/mol. Here again, the *b*-centrality

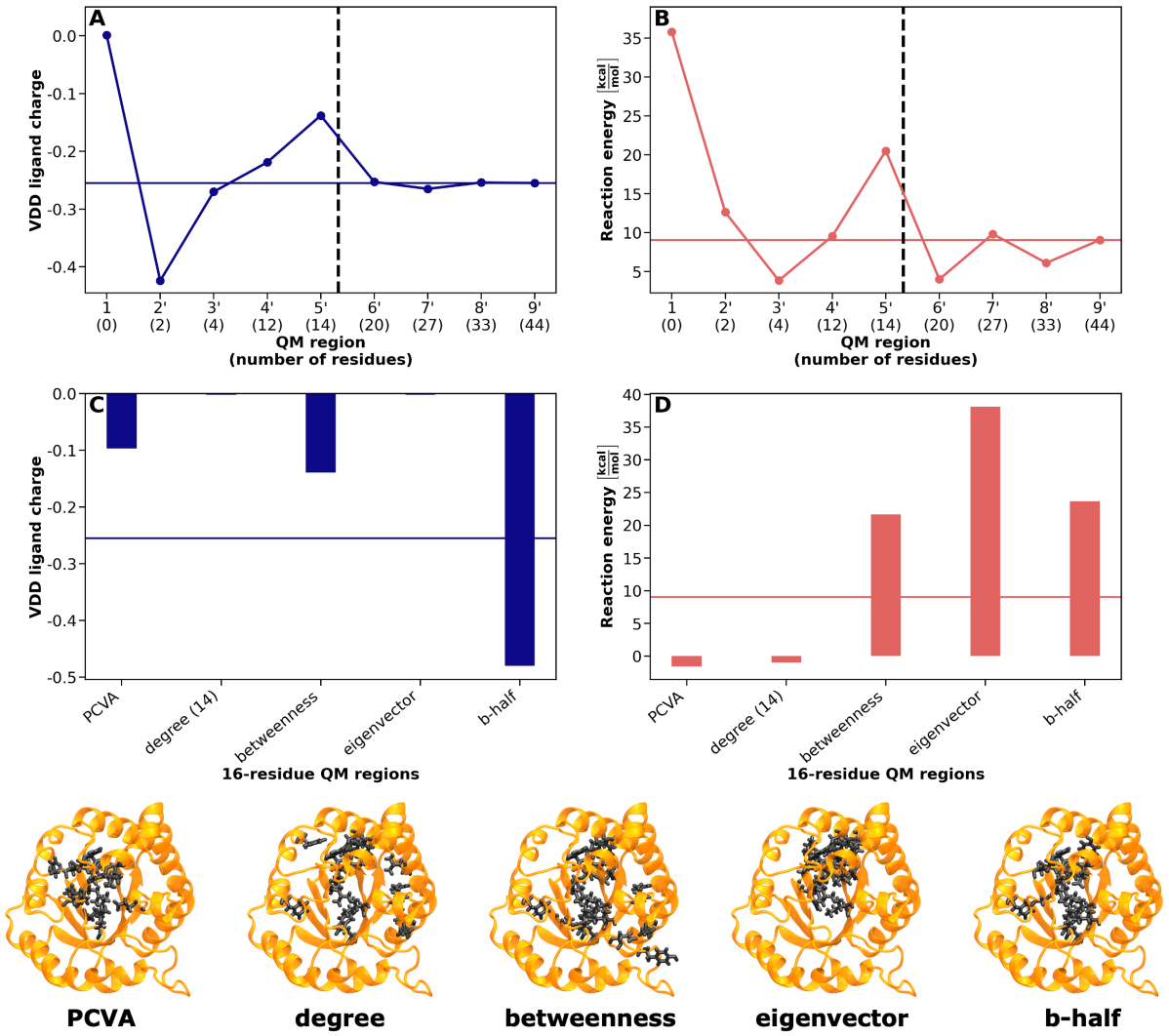

Figure S1: Ligand VDD charges and reaction energies from QM/MM calculations for TIM using QM regions of increasing size constructed using PCVA (upper part, adapted from Ref. [2]) and for atom-economical 16-residue QM regions constructed using PCVA as well as centrality-based descriptors (middle part). In the bottom part, the different QM regions are visualized without ligands. A: Convergence of the DHAP ligand VDD charges with increasing QM region size. B: Convergence of the QM/MM reaction energy for the interconversion reaction from DHAP to PGH in TIM with increasing QM region size. Best estimate results (corresponding to QM region **9'**) are indicated by a solid horizontal line. C: DHAP ligand VDD charge for atom-economical 16-residue QM regions (indicated by dashed vertical line in A) constructed using different centrality-based descriptors. D: QM/MM reaction energies for atom-economical 16-residue QM regions (indicated by dashed vertical line in B) constructed using different centrality-based descriptors.

performs best with about 22 kcal/mol, and the result is not improved by a combination with PCVA (about 24 kcal/mol).

Especially considering the previously discussed difficulties for TIM with non-detected high-impact residues such as HIS95 and the insufficient size of atom-economical QM regions (see Ref. 2), the observation that using the *b*-centrality moves both ligand charges and the reaction energy in the right direction is encouraging, and our results for TIM are thus a promising starting point for further investigations.

Table S5: Comparison of residues included in a 16-residue (14 for *d*-centrality) QM region of TIM using PCVA, using *d*-, *b*-, and *e*-centrality descriptors, and using the mixed *b-half* approach. Numbers indicate the rank of the amino acid according to different descriptors. The highest-ranked 16 residues are marked in red. Residues in the *d*-centrality ranking can have the same rank if they are assigned the same centrality value. For the mixed approach, 16 residues are assigned to their detection method indicated by b for *b*-centrality and by p for PCVA.

Residue	PCVA	d	b	e	b-half
PHE6	56	30	36	13	—
ASN10	12	66	79	67	—
LYS12	3	96	11	130	p
VAL39	113	15	10	31	—
ASN65	80	96	16	123	—
TYR67	152	30	13	191	—
TRP90	158	4	1	22	b
ILE92	75	44	8	54	b
HIS95	17	66	23	77	—
GLU97	13	139	32	165	—
ARG99	127	4	9	66	—
LYS112	148	8	14	80	—
THR113	233	10	41	53	—
ILE124	71	10	5	12	b
LEU147	128	10	24	34	—
VAL162	61	30	15	10	—

ALA163	23	66	65	15	—
TYR164	34	1	3	5	b
GLU165	5	66	50	44	p
ILE170	14	120	55	180	—
GLY171	9	240	244	239	p
HIS185	54	4	42	2	—
ILE188	91	15	49	11	—
ARG189	116	1	12	4	—
ARG205	90	15	4	8	b
ILE206	60	15	72	3	—
LEU207	31	10	19	1	—
TYR208	16	4	6	6	b
GLY209	6	139	77	45	p
GLY210	4	190	157	73	p
SER211	1	171	122	84	p
ALA212	7	66	67	52	p
ASN213	15	171	166	156	—
PHE220	42	10	22	33	—
VAL226	46	30	81	9	—
ASP227	66	15	57	7	—
GLY228	38	96	96	16	—
LEU230	8	8	2	14	b
VAL231	11	15	43	32	—
GLY232	10	120	114	96	—
GLY233	2	139	149	131	p
PHE240	58	3	7	38	b

Table S6: Information on the QM regions of increasing size for TIM constructed by PCVA with a variation of −0.5. Reproduced from *Phys. Chem. Chem. Phys.* **25**, 14484–14495 (2023), DOI: 10.1039/D3CP01263H.

Region	Charge	Residues	Link atoms	Included residues
1	0	0	0	DHAP/PGH
2	0	2	4	S211 G233 *
3	1	4	6	S211 G233 K12 G210 *
4	0	12	12	S211 G233 K12 G210 E165 G209 A212 L230 G171 G232 V231 N10 *
5	-1	14	14	S211 G233 K12 G210 E165 G209 A212 L230 G171 G232 V231 N10 E97 I170 *
6	-1	20	20	S211 G233 K12 G210 E165 G209 A212 L230 G171 G232 V231 N10 E97 I170 N213 Y208 H95 G173 A169 A175 *
7	-1	27	28	S211 G233 K12 G210 E165 G209 A212 L230 G171 G232 V231 N10 E97 I170 N213 Y208 H95 G173 A169 A175 N14 F229 A163 A234 P166 C216 L236 *
8	-1	33	28	S211 G233 K12 G210 E165 G209 A212 L230 G171 G232 V231 N10 E97 I170 N213 Y208 H95 G173 A169 A175 N14 F229 A163 A234 P166 C216 L236 G8 F11 I243 L207 L13 A176 *
9	-1	44	30	S211 G233 K12 G210 E165 G209 A212 L230 G171 G232 V231 N10 E97 I170 N213 Y208 H95 G173 A169 A175 N14 F229 A163 A234 P166 C216 L236 G8 F11 I243 L207 L13 A176 Y164 A217 Q64 G214 G228 Y101 S96 V7 F220 L174 A181 *

* + DHAP in reactants or PGH in products, respectively

Table S7: Information on the atom-economical, 16-residue QM regions constructed for TIM based on PCVA schemes, centrality descriptors and mixed approaches. Residues are ordered according to their position in the indicator ranking. Remark: degree consists of 14 residues.

Region	Charge	Residues	Link atoms	Included residues
PCVA	-1	16	14	S211 G233 K12 G210 E165 G209 A212 L230 G171 G232 V231 N10 E97 I170 N213 Y208 *
degree	3	14	24	R189 Y164 F240 Y208 H185 R99 W90 L230 K112 F220 L207 L147 I124 T113 *
betweenness	5	16	32	W90 L230 Y164 R205 I124 Y208 F240 I92 R99 V39 K12 R189 Y67 K112 V162 N65 *
eigenvector	1	16	16	L207 H185 I206 R189 Y164 Y208 D227 R205 V226 V162 I188 I124 F6 L230 A163 G228 *
b-half	1	16	22	W90 L230 Y164 R205 I124 Y208 F240 I92 S211 G233 K12 G210 E165 G209 A212 G171 *

* + DHAP in reactants or PGH in products, respectively

References

[1] F. Brandt and Ch. R. Jacob, Systematic QM Region Construction in QM/MM Calculations Based on Uncertainty Quantification, *J. Chem. Theory Comput.*, 2022, **18**, 2584–2596.

[2] F. Brandt and Ch. R. Jacob, Efficient automatic construction of atom-economical QM regions with point-charge variation analysis, *Phys. Chem. Chem. Phys.*, 2023, **25**, 14484–14495.

[3] D. Van Der Spoel, E. Lindahl, B. Hess, G. Groenhof, A. E. Mark, and H. J. C. Berendsen, GROMACS: Fast, flexible, and free, *J. Comput. Chem.*, 2005, **26**, 1701–1718.

[4] GROMACS Version 2019.6, 2020, DOI: 10.5281/zenodo.3685922, URL: http://www.gromacs.org/.

[5] K. Lindorff-Larsen, S. Piana, K. Palmo, P. Maragakis, J. L. Klepeis, R. O. Dror, and D. E. Shaw, Improved side-chain torsion potentials for the Amber ff99SB protein force field, *Proteins: Struct., Funct., Bioinf.*, 2010, **78**, 1950–1958.

[6] J. Wang, R. M. Wolf, J. W. Caldwell, P. A. Kollman, and D. A. Case, Development and testing of a general amber force field, *J. Comput. Chem.*, 2004, **25**, 1157–1174.

[7] J. Wang, W. Wang, P. A. Kollman, and D. A. Case, Automatic atom type and bond type perception in molecular mechanical calculations, *J. Mol. Graphics Model.*, 2006, **25**, 247–260.

[8] A. W. Sousa da Silva and W. F. Vranken, ACPYPE - AnteChamber PYthon Parser interfacE, *BMC Research Notes*, 2012, **5**, 367.

[9] ACPYPE, 2021, URL: https://github.com/alanwilter/acpype.

[10] H. J. Kulik, J. Zhang, J. P. Klinman, and T. J. Martínez, How Large Should the QM Region Be in QM/MM Calculations? The Case of Catechol O-Methyltransferase, *J. Phys. Chem. B*, 2016, **120**, 11381–11394.

[11] W. L. Jorgensen, J. Chandrasekhar, J. D. Madura, R. W. Impey, and M. L. Klein, Comparison of simple potential functions for simulating liquid water, *J. Chem. Phys.*, 1983, **79**, 926–935.

[12] R. C. Davenport, P. A. Bash, B. A. Seaton, M. Karplus, G. A. Petsko, and D. Ringe, Structure of the triosephosphate isomerase-phosphoglycolohydroxamate complex: an analog of the intermediate on the reaction pathway, *Biochemistry*, 1991, **30**, 5821–5826.

[13] Software for Chemistry and Materials, Amsterdam, AMS, Amsterdam Modelling Suite, 2020, URL: http://www.scm.com.

[14] G. te Velde, F. M. Bickelhaupt, E. J. Baerends, C. Fonseca Guerra, S. J. A. van Gisbergen, J. G. Snijders, and T. Ziegler, Chemistry with ADF, *J. Comput. Chem.*, 2001, **22**, 931–967.

[15] J. P. Perdew, K. Burke, and M. Ernzerhof, Generalized Gradient Approximation Made Simple, *Phys. Rev. Lett.*, 1996, **77**, 3865.

[16] E. Van Lenthe and E. J. Baerends, Optimized Slater-type basis sets for the elements 1-118, *J. Comput. Chem.*, 2003, **24**, 1142–1156.

[17] A. D. Becke, Density-functional thermochemistry. III. The role of exact exchange, *J. Chem. Phys.*, 1993, **98**, 5648–5652.

[18] P. J. Stephens, F. J. Devlin, C. F. Chabalowski, and M. J. Frisch, Ab Initio Calculation of Vibrational Absorption and Circular Dichroism Spectra Using Density Functional Force Fields, *J. Phys. Chem.*, 1994, **98**, 11623–11627.

[19] W. D. Cornell, P. Cieplak, C. I. Bayly, I. R. Gould, K. M. Merz, D. M. Ferguson, D. C. Spellmeyer, T. Fox, J. W. Caldwell, and P. A. Kollman, A Second Generation Force Field for the Simulation of Proteins, Nucleic Acids, and Organic Molecules, *J. Am. Chem. Soc.*, 1995, **117**, 5179–5197.

[20] E. Bitzek, P. Koskinen, F. Gähler, M. Moseler, and P. Gumbsch, Structural Relaxation Made Simple, *Phys. Rev. Lett.*, 2006, **97**, 170201.

[21] Software for Chemistry and Materials, Hybrid Engine Manual — Hybrid 2020 documentation, 2020, URL: https://www.scm.com/doc.2020/Hybrid/index.html.

[22] C. Fonseca Guerra, J.-W. Handgraaf, E. J. Baerends, and F. M. Bickelhaupt, Voronoi deformation density (VDD) charges: Assessment of the Mulliken, Bader, Hirshfeld, Weinhold, and VDD methods for charge analysis, *J. Comput. Chem.*, 2004, **25**, 189–210.

[23] A. T. Van Wart, J. Durrant, L. Votapka, and R. E. Amaro, Weighted Implementation of Suboptimal Paths (WISP): An Optimized Algorithm and Tool for Dynamical Network Analysis, *J. Chem. Theory Comput.*, 2014, **10**, 511–517.

[24] A. A. Hagberg, D. A. Schult, and P. J. Swart In ed. G. Varoquaux, T. Vaught, and J. Millman, *Proceedings of the 7th Python in Science Conference (SciPy2008)*, pp. 11–15, Pasadena, CA USA, 2008.

[25] NETWORKX Version 2.6.3, 2021, URL: https://networkx.org.

[26] J. D. Hunter, Matplotlib: A 2D Graphics Environment, *Comput. Sci. Eng.*, 2007, **9**, 90–95.

[27] MATPLOTLIB Version 3.4.2, 2021, DOI: 10.5281/zenodo.4743323, URL: https://matplotlib.org.

[28] W. Humphrey, A. Dalke, and K. Schulten, VMD — Visual Molecular Dynamics, *J. Mol. Graphics*, 1996, **14**, 33–38.